Neural Hybrid Automata: Learning Dynamics with Multiple Modes and Stochastic Transitions

Michael Poli[1,3,*], **Stefano Massaroli**[2,*], **Luca Scimeca**[3], **Seong Joon Oh**[3],
Sanghyuk Chun[3,4], **Atsushi Yamashita**[2], **Hajime Asama**[2], **Jinkyoo Park**[1], **Animesh Garg**[5,6]

Abstract

Effective control and prediction of dynamical systems often require appropriate handling of continuous–time and discrete, event–triggered processes. Stochastic hybrid systems (SHSs), common across engineering domains, provide a formalism for dynamical systems subject to discrete, possibly stochastic, state jumps and multi–modal continuous–time flows. Despite the versatility and importance of SHSs across applications, a general procedure for the explicit learning of both discrete events and multi–mode continuous dynamics remains an open problem. This work introduces *Neural Hybrid Automata* (NHAs), a recipe for learning SHS dynamics without *a priori* knowledge on the number of modes and inter-modal transition dynamics. NHAs provide a systematic inference method based on normalizing flows, neural differential equations and self–supervision. We showcase NHAs on several tasks, including mode recovery and flow learning in systems with stochastic transitions, and end–to–end learning of hierarchical robot controllers.

1 Introduction

Behaviors emerging from the interaction of continuous and discrete–time dynamics in the presence of uncertainty are described through the language of *stochastic hybrid systems* (SHSs). Such discrete events can bring along abrupt changes in the state, and in complex *multi–mode* systems, may also cause a *switch* between system *modes*, and corresponding underlying continuous dynamics [1]. Communication networks [2], [3], where changes in communication protocol can happen at certain levels of traffic congestion, and biological systems [4]–[6] are example domains where the SHS modeling paradigm has proven fruitful.

Data–driven identification and learning of hybrid systems are known to be challenging due to the entanglement of continuous flows and discrete events [7]; finding a generally applicable technique remains an open problem, particularly in the common scenarios where no *a priori* knowledge on the number and type of *system modes* is given. The aim of this work is to apply continuous neural models [8]–[10] to the learning SHSs. We introduce a compact descriptive language for this task, decomposing the system into a set of core primitives. Prior work is integrated into the framework, highlighting in the process limiting assumptions and areas of further improvement.

To address the shortcomings of existing techniques, we introduce *Neural Hybrid Automata* (NHA) as a general procedure designed to enable learning and simulation of SHSs from data. NHAs are comprised of three components: a dynamics module, taking the form of an *neural differential equation* (NDE) [8]–[10] capable of approximating a different vector field for each mode, a discrete latent state tracking the internal mode of the target system, and an event module determining the time to next event. In particular, our approach does not require prior knowledge on the number of modes.

---

[*]Equal contribution. Author order was decided by flipping a coin. [1]KAIST [2]The University of Tokyo [3]NAVER AI Lab [4] Naver Clova [5]University of Toronto, Vector Institute [6]Nvidia. Corresponding author: *Michael Poli* (`poli_m@kaist.ac.kr`)

The synergy among NHA components ensures a broader range of applicability compared to previous attempts, which in example do not directly tackle multi–mode hybrid systems [11]–[14]. NHAs are shown to enable mode recovery and learning of systems with stochastic transitions, with additional applications in end–to–end learning of hierarchical robot controllers.

2 Background

We introduce required background on the formalism of *stochastic hybrid systems* (SHSs) and event handling for their numerical simulation. We then provide further contextualization on previous approaches, introducing in the process a unified language for SHS learning tasks.

2.1 Stochastic Hybrid Systems

A *stochastic hybrid system* (SHS) [2], [15] is a right-continuous stochastic process X_t taking values in $\mathbb{X} \subseteq \mathbb{R}^{n_x}$ with a *latent mode* process Z_t conditioning the dynamics of X_t, where $t \geq 0$. Z_t is another right-continuous stochastic process that takes values in a finite set $\mathbb{M}$ of size m. In this context, the set $\mathbb{M}$ contains *identifiers* of internal system *modes*. An *event* is defined as either a mode switch or a state discontinuity (a *jump* in X_t), which can in some cases occur simultaneously. We refer to times at which events $z \to z'$ occur as random variables $t_k \in \mathcal{T}$, with associated *intensity functions* [16]

$$\lambda_{z \to z'}(t|\mathcal{H}_t) \geq 0.$$

where $\mathcal{H}_t := \{t_k \in \mathcal{T} : t_k < t\}$ is the *history* of event times. Intensity, as defined in the classical *temporal point process* (TPP) sense, can be interpreted as the expected number of events $z \to z'$ within the time interval $[t, t + \mathrm{d}t]$. The dynamics for X_t when $Z_t = z$ is defined by

$$\text{flow dynamics}: \quad \dot{x}_t = F_z(t, x_t). \qquad (z, t, x_t) \in \mathbb{M} \times \mathbb{T} \times \mathbb{X}$$

When a jump event $z \to z'$ is triggered, X_t can instantaneously jump according to

$$\text{jump dynamics}: \quad x_t^+ = \psi_{z \to z'}(t, x_t). \qquad (z, z', t, x_t) \in \mathbb{M}^2 \times \mathbb{T} \times \mathbb{X}$$

Jump maps $\psi_{z \to z'}$ and intensities $\lambda_{z \to z'}$ describe the behavior during events $z \to z'$.

2.2 Event Handling for Hybrid Systems

Following [17], to enable forward simulation of SHSs, a convenient mathematical representation of an *event* is a function $g : \mathbb{T} \times \mathbb{X} \to \mathbb{R}$ which nullifies only at any *event time* t^*, thus providing the differential equation integration algorithm with a *termination* or *restart* condition i.e.

$$t^* \text{ is an event} \iff g(t^*, x_{t^*}) = 0. \qquad (2.1)$$

The particular form of g induces a jump set on $\mathbb{D} \subset \mathbb{T} \times \mathbb{X}$, $\mathbb{D} := \{t, x : g(t, x_t) = 0\}$, and determines transitions from roots of g to regions of the state–space $\mathbb{X}$ where $g \neq 0$. Notably, this construct enables utilization of root finding methods [18] in a neighborhood of t^* to accurately zero in on the event time.

The same simulation technique can be extended to the *many* jump sets case typical of multi–mode systems, by equipping the condition function with identifiers z, z' ($g_{z \to z'}$) which induces jump sets $\mathbb{D}_{z \to z'}$.

Simulating stochastic events While the event function approach appears to be limited to the deterministic setting, it also subsumes stochastic events whose aleatoric uncertainty is encoded by an intensity $\lambda(t|\mathcal{H}_t)$ [1], [13]. Without loss of generality let us consider a single intensity function which is henceforth denoted as $\lambda_t^* := \lambda(t|\mathcal{H}_t)$. Recalling that the *cumulative distribution function* (CDF) of inter–event times is $1 - \exp\left\{-\int_{t_0}^{t^*} \lambda_t^* \mathrm{d}t\right\}$, standard *inverse transform sampling* [1], [19] yields

$$t^* : 0 = s - \log \int_{t_0}^{t^*} \lambda_t^* \mathrm{d}t, \quad s \sim \texttt{Uniform}(0, 1) \qquad (2.2)$$

as a special case of (2.1). Approaches developed for learning TPPs, including in the context of Neural ODEs [8], [11], [20], introduce a parametric formulation for the intensity λ_θ^* and optimize via direct TPP likelihood objectives. The integral is in general intractable, thus these methods require either a numerical approximation or the augmentation of additional states to compute it alongside the ODE.
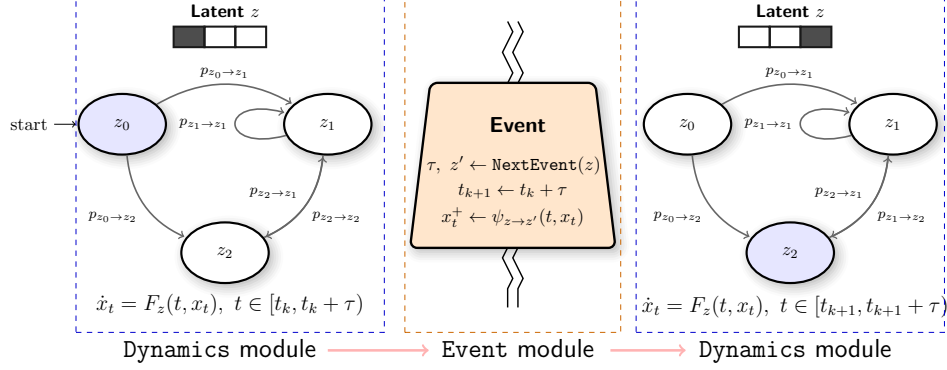
2

Figure 1: Schematic of a Neural Hybrid Automata (NHA). The mode–conditioned Neural ODE F_z drives the system forward until an event time t_{k+1} determined by a previous call to the event module. Then, the event module determines time to next event and corresponding mode target z' through sampling from normalizing flow $p_{z \to z'}$ approximating densities of interevent times. A jump function is then applied to the state x, and simulation continues with flow $F_{z'}$.

2.3 Core primitives for SHS learning

At minimum, a learning model for SHSs necessitates several modules, each mirroring an element of the formulation in 2.1. More specifically:

    i. Dynamics module, to approximate continuous dynamics F_z conditioned on mode z.

    ii. Discrete latent selector, to identify at each event time the latent mode z of the system.

    iii. Event module, to determine *when* events happen, and how state x and latent state z are updated after the transition.

Prior work considers specific instantiations of SHSs, leading to simplifying choices for each module defined above. In example, switching systems without jumps, where *iii.* does not require jumps [21], single mode systems, where *ii.* is not required and *iii.* does not need to determine latent mode transitions [11], [13], [14], systems with known dynamics, where *i.* is not trained [13], or systems with only deterministic events [7]. We note some of these works suffer from more than a single of these limitations, including additional ones consequence of specific model choices. Direct parametrization of the intensity, while a reasonable choice for single mode systems, requires state augmentation scaling in the worst case as $\binom{m}{2}$ [22] for a SHS with m modes. More importantly, training parameters θ for such direct approaches is affected by the accuracy of the numerical method employed for the solution of the integral in (2.2).

In this work, we introduce a modelling framework SHSs that does not rely on any of the simplifying assumption on *i.*, *ii.* and *iii.* outlined above. Furthermore, our method scales as $O(m)$ in the number of SHS modes.

3 Neural Hybrid Automata

We introduce *Neural Hybrid Automata* (NHA), a model for learning of SHSs. A NHA is comprised of a dynamics module, a discrete latent state and an event predictor. A general overview of a NHA is depicted in Figure 1. We start with a description of each module and their interconnections, followed by a step–by–step procedure for NHA training.

Event module Intensity–free parametrizations for stochastic mode transitions allows NHAs to sample next event times without solving integrals $\int \lambda_t^* \mathrm{d}t$ for all target modes z' reachable from current z. From event k at time t_k, NHAs determine next event times t_{k+1} through a conditional normalizing flow modeling, for each possible pair of (z, z'), the density of corresponding *inter–event* times $\tau_{z \to z'}^k = t_{k+1} - t_k, t_k \in \mathcal{T}_{z \to z'}$. Let the intensity be a simple *timer* i.e $\lambda = 1$. Further, let $p_{z \to z'}$ be the parametrized conditional density obtained by the normalizing flow and let $T(z, z', t_k)$ be a collection of conditional samples from $p_{z \to z'}$ (one for each pair z, z'), i.e.

$$T(z, z', t_k) = \left\{ \tau_{z \to z'}^k \sim p_{z \to z'}(\tau | \mathcal{H}_{t_k}) \right\}_{z, z' \in \mathbb{Z}}.$$
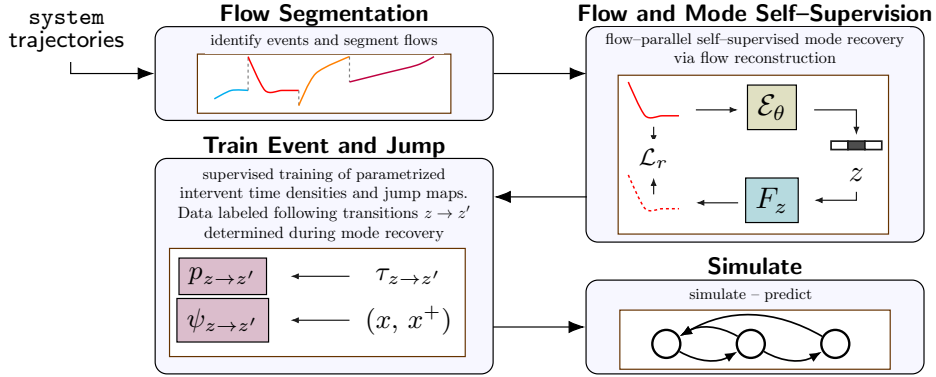
3

Figure 2: NHA training blueprint. Segmenting the trajectories enables self–supervised mode recovery via trajectory reconstruction. The recovered mode labels are then used for NHA event module supervised training.

Using (2.2), we can thus sample an event given the current mode z and the previous event time t_k as:

$$t_{k+1} = t_k + \min_{z' \in \mathbb{Z}} T(z, z', t_k). \tag{3.1}$$

Note that the next mode z' after the event is simultaneously obtained as $z' = \arg\min T(z, z', t_k)$. Sampling strategy (3.1), differently from (2.2), relies on the normalizing flow to explicitly model the density rather than defining it implicitly through $\int \lambda_t^* \mathrm{d}t$. When event time t_k is reached, a parametrized jump map conditioned on (z, z') is applied to the state $x^+ = \psi_{z \to z'}(t_k, x)$. Normalizing flow $p_{z \to z'}$ and jump map $\psi_{z \to z'}$ together define the full event module of an NHA.

It should be noted that (3.1) always samples the *quickest–to–occur* event from the normalizing flow, which implies that no other event occurs between t_k and t_{k+1}. While the history can be compressed into a fixed–length vector following [23] through application of sequence models e,g. RNNs, we note that for hybrid systems equipped with deterministic events, providing (x_{t_k}, t_k) as conditioning inputs for $p_{z \to z'}(\tau)$ is sufficient since ODE solutions with deterministic transitions are uniquely determined by the initial condition. Finally, deterministic events are a special case of stochastic events [2] that can be well–represented with a Dirac δ function, of which the normalizing flow learns a smooth approximation with continuous support.

Dynamics module   To enable approximation of different mode–dependent vector fields, we parametrize the *flow map* $F_z(t, x_t)$ of a SHS as a *data–controlled neural ordinary differential equation* (Neural ODE) [9] with parameters ω, driven between each pair of event times t_k, t_{k+1} by discrete latent mode z

$$\dot{x}_t = F_z(t, x_t, \omega) \qquad t \in [t_k, t_{k+1}) \tag{3.2}$$

Finiteness of admissible values in the latent mode state i.e. m ensures F is capable of approximating a finite number of different vector fields, one for each mode. In particular, we consider one–hot representations for latents $z \in \mathbb{R}^m$. In batched data settings, (3.2) can be integrated in parallel across n_b batches of initial conditions $x_{t_k} \in \mathbb{R}^{n_b \times n_x}$ with different modes, provided the latent is also batched $z \in \mathbb{R}^{n_b \times m}$. The combination of a given dynamics and event module, applied in turn as depicted in Figure 1, enables simulation of trajectories of a SHS. We now describe their training procedure.

4   Neural Hybrid Automata Module Training

Here, we detail the training procedure for each NHA component. Our only assumption is availability to a *trajectory segmentation* routine tasked with separating the trajectories, or flows, into a collection of *subtrajectories* X_i of potentially of different length, each produced by the system in a different mode. The routine can be as simple as detection of discontinuities in the solution by inspecting *finite–differences* of observations across timestamps [24], or involve additional steps such as change–point detection [25]. Providing exact event times to NHAs is not required; the segmentation routine need only partition the full dataset in n disjoint sets X_i s.t. $\bigcup_i X_i = X$ and $\bigcap_i X_i = \emptyset$. In addition, no knowledge of the number of modes, or topology of transitions between modes is made available to NHAs, as these are rarely available in practice.

4

Self–supervised mode recovery   The first stage of learning an NHA is designed to approximate the continuous dynamics under each SHS mode while simultaneously identifying modes z. We achieve this by framing subtrajectory reconstruction as a *pretext* task for mode recovery, via a reconstruction objective $\mathcal{L}_r = \frac{1}{n} \sum_{i=0}^{n} \ell_r(X_i, \hat{X}_i)$, being $\hat{X}_i$ subtrajectories reconstructed by the flow decoder F_z via the model

$$
\begin{aligned}
z &\sim \mathcal{E}(X, \theta) & t &= t_k \\
\dot{x} &= F_z(t, x_t, \omega) & t &\in [t_k, t_{k+1}).
\end{aligned}
\tag{4.1}
$$

Here, a latent *encoder* $\mathcal{E}$ with parameters θ is tasked with extracting a latent mode state $z \in \mathbb{M}$ to steer the decoder F_z towards a more accurate reconstruction. Representation limitations of Neural ODEs [9], [26] ensure that to fit the above objective the the encoder $\mathcal{E}$ has to cluster the trajectories to enable the data–control decoder to represent different vector fields for each system mode. Finiteness of admissible values in the latent state is enforced by defining z as one–hot encoded sample from a parametrized categorical distribution. Backpropagating through the sampling procedure is performed via straight–through gradients [27]. System (4.1) can be regarded as an ODE trajectory autoencoder with a categorical bottleneck.

Finally, we note that trajectory segmentation serves multiple purposes during NHA training. Forward integration is significantly sped up since the ODE solves can now be parallelized across subtrajectories X_i as independent samples of a batch of data, avoiding a sequential solve on full SHS trajectories. The speedups can be dramatic for multi–mode SHSs[2], the focus of this work, where data trajectories may need to be longer to sufficiently *explore* different modes.

Event and jump supervision   In addition to the learning of mode dynamics, self–supervised mode recovery objectives provides direct supervision for normalizing flows $p_{z\to z'}$ and jump maps $\psi_{z\to z'}$. More specifically, we collect times $\tau_{z\to z'}^k$ and jump state pairs (x, x^+) for each pair of modes (z, z') corresponding to a transition between pairs of subtrajectories clustered as z (first) and z' (second) by the encoder $\mathcal{E}$. We then train the jump maps $\psi_{z\to z'}$ to approximate $x \mapsto x^+$, and the mode conditional normalizing flow to approximate the density $p_{z\to z'}(\tau)$.

Gradient pathologies in joint learning of flows and events   When attempting simultaneous learning on the full trajectory, the parameters of flow F_z can be subjected to wrong gradients from reconstruction objectives, arising from overreliance or underreliance of the flow model on certain modes. This phenomenon can bias training, and provides strong motivation behind our segmentation–first approach, since each subtrajectory X_i is associated only to a single mode[3].
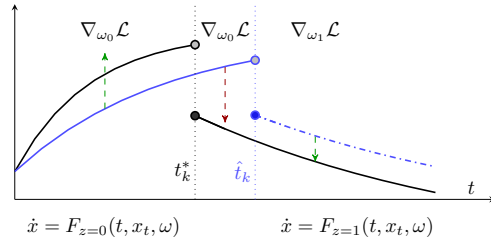

Figure 3: Conflicting gradient information in an idealized 2–mode hybrid system due to overestimation of event time.

A visualization is provided in Figure 3, through an idealized learning task of a two–mode system. Overreliance of the flow model on mode $z = 0$, due to overestimation of event time t_k, leads to a decomposition of gradients $\nabla_{w_0} \mathcal{L}_r$; in green, gradients pushing the trajectory closer to the solution, in red, incorrect gradients pushing the mode 0 trajectory further away from the ground–truth and closer to a solution belonging to a different mode. Appendix A further develops theoretical considerations on the nature of these gradients.

5   Results and Discussion

We evaluate *Neural Hybrid Automata* (NHA) through extensive experiments, with a focus on investigating the performance and robustness of each NHA module. A summary of experiments, objectives and ablations is provided here for clarity:

---

[2]While speedups are dependent on full trajectory and average subtrajectory lengths, in our experiment we observe at least an order of magnitude (more than 20x) in wall–clock speedups for a single training iteration.

[3]Due to inaccuracies or noise in the segmentation algorithm, these partitions might not be perfectly separated into different modes. We experimentally investigate these effects on NHA training in Appendix B.
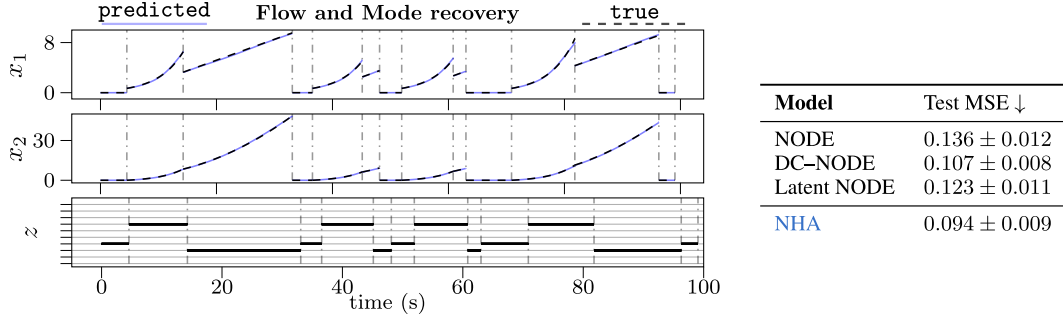
Figure 4: **[Left]** Reconstruction of system trajectories through NHA vector field decoders F_z and corresponding modes z encoded by $\mathcal{E}$ for Reno `TCP`. Although the encoder is initialized with more modes (10) than there are in the underlying system (3), mode clustering is sparse and accurate. **[Right]** Flow reconstruction test MSE for different classes of decoders. NHA decoders (10 modes) can reconstruct the flows as well as other NODE baselines, with the added benefit of being able to recover mode labels during training.

- **Reno TCP**: we carry out a quantitative evaluation on quality of learned flows (mean squared error) and quality of mode clusters recovered during self–supervision (v–measure). We also verify the robustness of NHAs to overclustering and amount of data required for event module training.

- **Mode mixing in switching systems**: we highlight and varify robustness against *mode mixing*, a phenomenon occurring during learning of multi–mode systems through alternative *soft* parametrization of latent z, such as through `softmax` instead of `categorical` samples.

- **Behavioral control of wheeled robots**: NHAs enable task–based behavioral control. We investigate a point–to–point navigation task where a higher level *reinforcement learning* (RL) planner determines mode switching for a lower–level optimal controller.

5.1 System with Stochastic Transitions

We apply NHAs to a dataset of internal state trajectories of a network transmission controller (TCP), the Reno TCP scheme [2]. The system has two states, five stochastic transitions and three modes as shown through an automata representation in Figure 5. Here, we qualitatively validate the performance of dynamics and event modules of NHAs. We simulate 40 trajectories of the system, each 200 seconds long, and segment them. No a priori knowledge on the mode of each subtrajectory is provided to the model. We perform self–supervised mode recovery to train F_z and $\mathcal{E}$, in the process labeling the subtrajectories, then train event module normalizing flows and jump

Figure 5: Automata representation of TCP Reno, where η, p_{drop}, $\kappa > 0$ and we set $n_{ack} = 2$. On each edge is the corresponding intensity $\lambda_{z \to z'}$.

functions with the mode labels obtained. Training and evaluation are performed using a 5–fold cross–validation strategy, with a final test fold of 15. More details on the system, architectures and data generation are reported in the Appendix B.

Mode recovery results First, we perform self–supervised mode recovery and verify (i) whether the mode conditioned NHA decoder F_z offers test–time TCP trajectory reconstruction of equal or better quality than other Neural ODE variants, and (ii) quality of the mode label clusters assigned by the NHA encoder and robustness to different number of latent modes m. We measure (i) via test *mean squared error* (MSE) on reconstructed trajectories, and (ii) via *v–measure* [28], a metric taking values in $[0, 1]$, computed as the harmonic mean between cluster *completeness* and *homogeneity*. A v–measure of 1 indicates perfect clustering. As baselines, we collect for (i) the performance of 3 *Neural ODE* (NODE) variants, a zero–augmented NODE, a *data–controlled NODE* (DC–NODE) [9] where the latent z is the output of a multi–layer encoder, and a Latent NODE where z is sampled via reparametrization of a Normal [8]. We also provide baseline performance of a series of popular clustering algorithms tasked to cluster the subtrajectories: k–means++ [29], hierarchical [30] and DBSCAN [31]. Figure 4 provides qualitative and quantitative results for stage (i). As established by 1, NHA mode recovery outperforms all baselines by a wide margin,
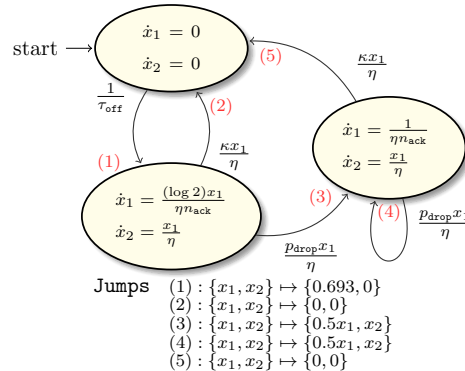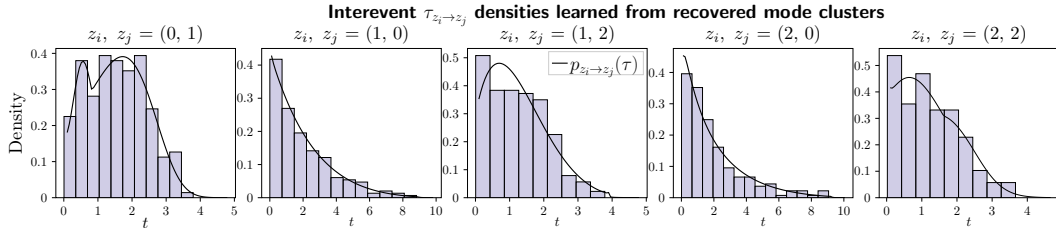
6

Figure 6: Learned densities (black) for intervent times $\tau_{z_i \to z_j}$. The normalizing flows are trained on times recovered during the mode recovery stage, by clustering $\tau_{z_i \to z_j}$ according to the encoder mode labeling. The histogram depicts the ground–truth empirical distribution for each class of event.

with v–measure values close to 1. Surprisingly, we observe providing the NHA encoder with a larger number of latent modes than the 3 of the system improves clustering results. Additional details on data pre–processing, metrics and baseline design and tuning are provided in Appendix B.

Event module results Next, we leverage the mode labels recovered as supervision for the event module of an NHA. In all cases, we train three–layer MLPs as jump maps and two–layer spline flows [32] as normalizing flows. Figure 6 visualizes the learned densities for each stochastic transition for the standard training regime of $n = 5$ trajectories. We also perform an ablative study on the quantity of data required to extract sufficient supervision signal for both components of the event module. The results are included in Table 1. We find that a single trajectory is sufficient, with relative performance gains quickly dropping off after $n = 3$.

	v–measure ↑		
Model	$m = 3$	$m = 5$	$m = 10$
k–means++	0.20 ± 0.02	0.24 ± 0.02	0.30 ± 0.06
hierarchical	0.23 ± 0.01	0.24 ± 0.01	0.31 ± 0.06
DBSCAN	0.66 ± 0.02	0.68 ± 0.02	0.69 ± 0.01
NHA	$\mathbf{0.86} \pm 0.02$	$\mathbf{0.91} \pm 0.02$	$\mathbf{0.96} \pm 0.03$

Table 1: Quality of recovered mode clusters from NHA self–supervised training and baseline clustering algorithms in the TCP task. Hyperparameter m is the number of clusters provided to each algorithm. For DBSCAN, values of $m \in [3, 5, 10]$ map instead to its primary parameter $\epsilon \in [0.1, 0.5, 1]$ [31].

Model	Metric	$n = 1$	$n = 3$	$n = 5$	$n = 10$
$p_{z \to z'}$	NLL ↓	2.761	2.375	2.362	2.313
$\psi_{z \to z'}$	MSE (10^{-3}) ↓	1.435	0.018	0.009	0.003

Table 2: Quality of fit for event module components, normalizing flows p and jump maps ψ. Training performed with supervising mode labels from n trajectories of TCP. We report test MSE and *negative log–likelihood* (NLL) estimated from a base normalizing flow model trained on ground–truth data from $n = 500$.

5.2 Deterministic Switching System

We investigate *mode mixing* in a three–mode switching linear system (SLS) [13]. The deterministic nature of mode transitions, as well as the absence of state jumps enables direct training of NHAs on data–trajectories without prior segmentation. This allows us to perform an ablative study on *mode mixing*, a phenomenon arising from latent modes z produced by the encoder $\mathcal{E}$ via *soft* alternatives to categorical samples, such as by using `softmax` activations.

Mode mixing and overclustering We train NHAs on reconstruction of SLS trajectories. Each encoder is provided, at initialization, one additional latent mode over the three of the system. The conditioned flow F_z is constructed with three–layer MLPs. Rather than segmenting the data, we repeat sampling for z at each integration step. Figure 7 shows the state space switching boundaries and mode vector fields learned by an NHA and a baseline producing z via `softmax` rather than as categorical samples. The additional freedom provided by softmax latents $z \in \mathbb{R}_+^4$, $\sum z_i = 1$ allows fitting the trajectories by nonlinearly mixing different vector fields to approximate a single one. Instead, categorical samples cannot mix the vector fields; this ensures that the learned clustering is either sparse as shown in the Fig.7, or latent values dedicated to the approximation of the same underlying mode dynamics are forced to learn the same vector field. Appendix B contains a visualization and analysis for this second case.

In general, categorical sampling is effective when recovery of system modes is a model objective, whereas `softmax` or other soft relaxations can be viable if only black–box fitting of data is desired.
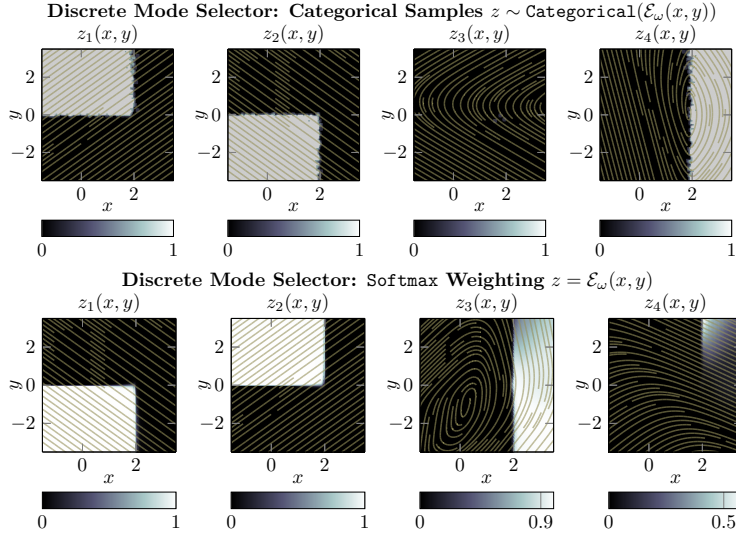
7

Figure 7: Reconstructed conditional vector fields F_z and corresponding mode classification boundaries in the state–space of the LSS. **[Above]** Categorical NHA encoder. **[Below]** Mode classification performed by "soft" encoder $\mathcal{E}$ capped with a `softmax` activation.

5.3 End–To–End Learning of Hierarchical Switching Controllers for Dynamical Systems

Beyond SHS identification, the NHA framework enables learning of task–based hierarchical controllers comprising a low–level controller $u_z := u(t, x_t, z)$ dependent on the discrete mode z provided by a higher–level policy π. Each NHA module is adapted as:

$$
\begin{aligned}
\text{dynamics module: } & \dot{x}_t = F(t, x_t, u_z)\mathrm{d}t && \text{low–level controlled system} \\
\text{event module: } & z' \leftarrow \pi(t, x_t, z) && \text{high–level planner}
\end{aligned}
\tag{5.1}
$$

Within this context, latent state z can be regarded as a system *set–point* (e.g. a desired value of state x) determined by the planning policy π to achieve a certain task, which the low–level controller has then to carry out. Both π and u_z are parametrized by neural networks, and the training is done end–to–end. The obtained hierarchical control scheme is sample efficient, since system dynamics available a priori are included in F. From the perspective of π, however, the dynamics are *disentangled* from the planning objective. Indeed, the higher level policy need only learn how to set and switch between objectives ($z \rightarrow z'$), and not how to control the system to reach them. For this reason we train the model using a loss function partitioned in two terms as $\mathcal{L} = \mathcal{L}_u + \mathcal{L}_\pi$.

Results We consider learning controllers for navigation of two-wheeled differential drive robots [33]. The higher–level model–free policy π is here trained via REINFORCE gradients [34], [35] to
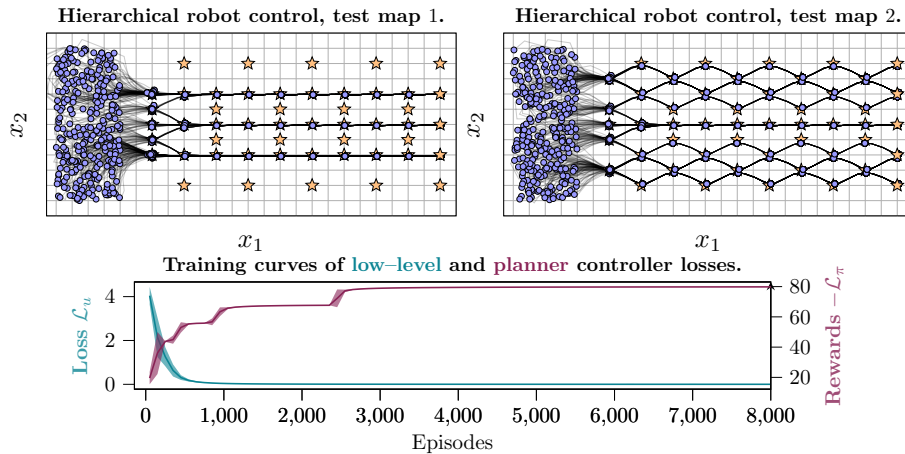

Figure 8: **[Above]**: Test–time learned navigation of swarms of differential drive robots. The robots are initialized at random locations and orientations. **[Below]**: Training loss curves of low–level controller u and planner π across episodes.

8

select the nearest resource target every 5 seconds. We set 5 different resources within a map, and train all robots to: one, select the nearest resource target; two, drive the wheels to reach the target. The training of both controllers is carried out concurrently, where target (or *mode*) selection is performed by π, whereas the behavioural controller u_z has to reach the target chosen by π via low–level steering control inputs. As shown in Figure 8, convergence of both control policies occurs after around 4000 episodes of training. Figure 8 also visualizes the resulting navigation behavior at test–time on two new resource layouts, where we alternate between two different sets of targets.

5.4 Generalizable Insights and Empirical Observations

The task of learning SHSs involves several moving components. Ablative experiments have been performed to address specific questions on the robustness of NHAs. We detail some empirical heuristics observed to improve performance, and report areas of further improvement.

• **Overclustering stabilizes training** We empirically observe providing NHA with more latent modes than the system stabilizes training. We conjecture the additional choice allows the model to use different modes during exploration without always conflicting with other already "assigned" modes, phenomenon which is more frequent, in example, when the number of modes exactly matches that of the system. In these cases, dropout in the encoder $\mathcal{E}$ appears to improve performance.

• **Noisy segmentation of trajectories** We investigate, for the TCP experiment, robustness of mode recovery to incorrect segmentation (Appendix B) and number of NHA latent modes m (Table 1). Extending NHAs to include a finetuning step for trajectory segmentation, in example leveraging ideas from [13] might improve robustness of the segmentation routine and thus the overall approach.

6 Related Work

Hybrid system identification and Markov models Hybrid system identification is a relatively recent development in dynamical system theory [7]. A majority of existing literature focuses on (linear) *piecewise affine systems* (PWA) [36], [37]. [38] proposes a clustered symbolic regression algorithm for learning input–output maps rather than dynamics. Existing approaches involving continuous optimization [21] do not consider event stochasticity and mode recovery. Identification of SHSs is an even smaller field, with limited success outside specific cases [15].

Continuous–depth and contact models Neural differential equations and continuous–depth models, initially concerned with unimodal systems [8], [9], have seen preliminary application to the learning of temporal point processes [11], [39]. Although some of these works tackle stochastic events and marked point processes, multimodality and explicit learning of the flows is not considered. [12] examine *interventions* as events, and develop a continuous architecture for modeling the lasting effect of a given intervention on the dynamics. Differentiable contact approaches [14], [40] introduce physics–compatible models designed to recover deterministic hybrid dynamics of mechanical systems from data. [13] develops, through implicit differentiation, a method for direct optimization of event times. Although Neural Event ODEs do not directly address multimodality, a potential synergy between the approach of [13] and NHAs could preserve the advantage of our flow–parallel mode recovery, namely integration speed and sidestepping of gradient pathologies outlined in Section IV. Section 2.3 provides a summary of limitations for these existing methods.

7 Conclusion

Hybrid systems represent a versatile and general class of systems, with applications across engineering disciplines [15]. In this work, we investigate challenges related to the learning of SHSs from data and introduce *Neural Hybrid Automata* (NHA), a step–by–step method leveraging neural differential equations, density estimation and self–supervised system mode recovery. NHAs are shown to be effective in various settings, including flow and event learning in systems with stochastic transitions.

References

[1] C. G. Cassandras and J. Lygeros, *Stochastic hybrid systems*. CRC Press, 2018.

[2] J. P. Hespanha, "Stochastic hybrid systems: Application to communication networks," in *International Workshop on Hybrid Systems: Computation and Control*, Springer, 2004, pp. 387–401.

[3] G. Sun, C. G. Cassandras, Y. Wardi, C. G. Panayiotou, and G. F. Riley, "Perturbation analysis and optimization of stochastic flow networks," *IEEE Transactions on Automatic Control*, vol. 49, no. 12, pp. 2143–2159, 2004.

[4] R Alur, C Belta, F Ivancic, V Kumar, M Mintz, G Pappas, H Rubin, J Schug, and G. Pappas, "Hybrid modeling and simulation of biological systems," *Hybrid Systems: Computation and Control*, vol. 2034, pp. 19–32, 2001.

[5] J. P. Hespanha and A. Singh, "Stochastic models for chemically reacting systems using polynomial stochastic hybrid systems," *International Journal of Robust and Nonlinear Control: IFAC-Affiliated Journal*, vol. 15, no. 15, pp. 669–689, 2005.

[6] X. Li, O. Omotere, L. Qian, and E. R. Dougherty, "Review of stochastic hybrid systems with applications in biological systems modeling and analysis," *EURASIP Journal on Bioinformatics and Systems Biology*, vol. 2017, no. 1, pp. 1–12, 2017.

[7] F. Lauer and G. Bloch, "Hybrid system identification," in *Hybrid System Identification*, Springer, 2019, pp. 77–101.

[8] T. Q. Chen, Y. Rubanova, J. Bettencourt, and D. K. Duvenaud, "Neural ordinary differential equations," in *Advances in neural information processing systems*, 2018, pp. 6571–6583.

[9] S. Massaroli, M. Poli, J. Park, A. Yamashita, and H. Asama, "Dissecting neural odes," *arXiv preprint arXiv:2002.08071*, 2020.

[10] C. Rackauckas, Y. Ma, J. Martensen, C. Warner, K. Zubov, R. Supekar, D. Skinner, and A. Ramadhan, "Universal differential equations for scientific machine learning," *arXiv preprint arXiv:2001.04385*, 2020.

[11] J. Jia and A. R. Benson, "Neural jump stochastic differential equations," in *Advances in Neural Information Processing Systems*, 2019, pp. 9843–9854.

[12] D. Gwak, G. Sim, M. Poli, S. Massaroli, J. Choo, and E. Choi, "Neural ordinary differential equations for intervention modeling," *arXiv preprint arXiv:2010.08304*, 2020.

[13] R. T. Chen, B. Amos, and M. Nickel, "Learning neural event functions for ordinary differential equations," *arXiv preprint arXiv:2011.03902*, 2020.

[14] Y. D. Zhong, B. Dey, and A. Chakraborty, "A differentiable contact model to extend lagrangian and hamiltonian neural networks for modeling hybrid dynamics," *arXiv preprint arXiv:2102.06794*, 2021.

[15] C. G. Cassandras and J. Lygeros, "Stochastic hybrid systems," *Automation and Control Engineering*, vol. 24, 2007.

[16] D. J. Daley and D. Vere-Jones, *An introduction to the theory of point processes: volume II: general theory and structure*. Springer Science & Business Media, 2007.

[17] L. Shampine and S Thompson, "Event location for ordinary differential equations," *Computers & Mathematics with Applications*, vol. 39, no. 5-6, pp. 43–54, 2000.

[18] J. Nocedal and S. Wright, *Numerical optimization*. Springer Science & Business Media, 2006.

[19] J. G. Rasmussen, "Temporal point processes: The conditional intensity function," *Lecture Notes, Jan*, 2011.

[20] R. T. Chen, B. Amos, and M. Nickel, "Neural spatio-temporal point processes," *arXiv preprint arXiv:2011.04583*, 2020.

[21] F. Lauer, G. Bloch, and R. Vidal, "A continuous optimization framework for hybrid system identification," *Automatica*, vol. 47, no. 3, pp. 608–613, 2011.

[22] D. B. West *et al.*, *Introduction to graph theory*. Prentice hall Upper Saddle River, 2001, vol. 2.

[23] O. Shchur, M. Biloš, and S. Günnemann, "Intensity-free learning of temporal point processes," *arXiv preprint arXiv:1909.12127*, 2019.

[24] S. Massaroli, F. Califano, A. Faragasso, M. Risiglione, A. Yamashita, and H. Asama, "Identification of a class of hybrid dynamical systems," *IFAC-PapersOnLine*, vol. 53, no. 2, pp. 875–882, 2020.

[25] S. Aminikhanghahi and D. J. Cook, "A survey of methods for time series change point detection," *Knowledge and information systems*, vol. 51, no. 2, pp. 339–367, 2017.

[26] E. Dupont, A. Doucet, and Y. W. Teh, "Augmented neural odes," in *Advances in Neural Information Processing Systems*, 2019, pp. 3134–3144.

[27] Y. Bengio, N. Léonard, and A. Courville, "Estimating or propagating gradients through stochastic neurons for conditional computation," *arXiv preprint arXiv:1308.3432*, 2013.

[28] A. Rosenberg and J. Hirschberg, "V-measure: A conditional entropy-based external cluster evaluation measure," in *Proceedings of the 2007 joint conference on empirical methods in natural language processing and computational natural language learning (EMNLP-CoNLL)*, 2007, pp. 410–420.

[29] D. Arthur and S. Vassilvitskii, "K-means++: The advantages of careful seeding," Stanford, Tech. Rep., 2006.

[30] F. Murtagh and P. Contreras, "Algorithms for hierarchical clustering: An overview," *Wiley Interdisciplinary Reviews: Data Mining and Knowledge Discovery*, vol. 2, no. 1, pp. 86–97, 2012.

[31] D. Birant and A. Kut, "St-dbscan: An algorithm for clustering spatial–temporal data," *Data & knowledge engineering*, vol. 60, no. 1, pp. 208–221, 2007.

[32] C. Durkan, A. Bekasov, I. Murray, and G. Papamakarios, "Neural spline flows," *arXiv preprint arXiv:1906.04032*, 2019.

[33] S. K. Malu and J. Majumdar, "Kinematics, localization and control of differential drive mobile robot," *Global Journal of Research In Engineering*, 2014.

[34] R. S. Sutton and A. G. Barto, *Reinforcement learning: An introduction*. MIT press, 2018.

[35] J. Peters and S. Schaal, "Policy gradient methods for robotics," in *2006 IEEE/RSJ International Conference on Intelligent Robots and Systems*, IEEE, 2006, pp. 2219–2225.

[36] S. Paoletti, A. L. Juloski, G. Ferrari-Trecate, and R. Vidal, "Identification of hybrid systems a tutorial," *European journal of control*, vol. 13, no. 2-3, pp. 242–260, 2007.

[37] R. L. Westra, M. P. Ralf, and L. Peeters, "Identification of piecewise linear models of complex dynamical systems," *IFAC Proceedings Volumes*, vol. 44, no. 1, pp. 14 863–14 868, 2011.

[38] D. L. Ly and H. Lipson, "Learning symbolic representations of hybrid dynamical systems," *The Journal of Machine Learning Research*, vol. 13, no. 1, pp. 3585–3618, 2012.

[39] Y. Rubanova, T. Q. Chen, and D. K. Duvenaud, "Latent ordinary differential equations for irregularly-sampled time series," in *Advances in Neural Information Processing Systems*, 2019, pp. 5321–5331.

[40] A. Hochlehnert, A. Terenin, S. Sæmundsson, and M. Deisenroth, "Learning contact dynamics using physically structured neural networks," in *International Conference on Artificial Intelligence and Statistics*, PMLR, 2021, pp. 2152–2160.

[41] A. L. Mitchell, M. Engelcke, O. P. Jones, D. Surovik, S. Gangapurwala, O. Melon, I. Havoutis, and I. Posner, "First steps: Latent-space control with semantic constraints for quadruped locomotion," in *2020 IEEE/RSJ International Conference on Intelligent Robots and Systems (IROS)*, IEEE, 2020, pp. 5343–5350.

[42] Y. D. Zhong and N. Leonard, "Unsupervised learning of lagrangian dynamics from images for prediction and control," *Advances in Neural Information Processing Systems*, vol. 33, 2020.

[43] A. M. Johnson, S. A. Burden, and D. E. Koditschek, "A hybrid systems model for simple manipulation and self-manipulation systems," *The International Journal of Robotics Research*, vol. 35, no. 11, pp. 1354–1392, 2016.

[44] P. Holmes, R. J. Full, D. Koditschek, and J. Guckenheimer, "The dynamics of legged locomotion: Models, analyses, and challenges," *SIAM review*, vol. 48, no. 2, pp. 207–304, 2006.

[45] J. Deng, W. Dong, R. Socher, L.-J. Li, K. Li, and L. Fei-Fei, "Imagenet: A large-scale hierarchical image database," in *2009 IEEE conference on computer vision and pattern recognition*, Ieee, 2009, pp. 248–255.

[46] E. Bingham, J. P. Chen, M. Jankowiak, F. Obermeyer, N. Pradhan, T. Karaletsos, R. Singh, P. Szerlip, P. Horsfall, and N. D. Goodman, "Pyro: Deep universal probabilistic programming," *The Journal of Machine Learning Research*, vol. 20, no. 1, pp. 973–978, 2019.

[47] F. Pedregosa, G. Varoquaux, A. Gramfort, V. Michel, B. Thirion, O. Grisel, M. Blondel, P. Prettenhofer, R. Weiss, V. Dubourg, *et al.*, "Scikit-learn: Machine learning in python," *the Journal of machine Learning research*, vol. 12, pp. 2825–2830, 2011.

[48] J. R. Dormand and P. J. Prince, "A family of embedded runge-kutta formulae," *Journal of computational and applied mathematics*, vol. 6, no. 1, pp. 19–26, 1980.

Neural Hybrid Automata
Supplementary Material

Table of Contents

A Additional Discussion and Theory

A.1 Neural Hybrid Automata: Modules and Hyperparameters

We provide a notation and summary table for *Neural Hybrid Automata* (NHA). The table serves as a quick reference for the core concepts introduced in the main text.

1. Dynamics: tasked with approximating continuous dynamics of each mode by conditioning a Neural ODE on mode z.

2. Mode Encoder: only used during self–supervised mode recovery. Labels every subjtrajectory X_i with a mode z to ensure mode–conditioned decoder F_z can reconstruct it despite Neural ODE representation limitations (uniqueness of solutions given an initial condition).

3. Event Module: determines during simulation (i) when events happen, and what types of events i.e. mode transitions $(z \to z')$ through $p_{z \to z'}$, (ii) what happens during such events i.e. jumps on the state via $\psi_{z \to z'}$. Normalizing flow $p_{z \to z'}$ is trained to approximate densities $p(\tau_{z \to z'} | \mathcal{H})$.

The only NHA hyperparameter beyond module architectural choices is m, or number of latent modes provided to the model at initialization. Performance effects of changing m have been explored in Section 5.2 and Appendix B.2. Appendix B.2 further provides analyzes potential techniques to prune additional modes.

A.2   Gradient Pathologies

We provide some theoretical insights on the phenomenon of gradient pathologies with the simple example of a one–dimensional linear hybrid system with two modes and one *timed* jump,

$$
\begin{aligned}
\dot{x}_t &= \begin{cases} ax_t & t < \tau \\ bx_t & t >= \tau \end{cases} \qquad t \neq \tau \\
x_t^+ &= cx_t \qquad\qquad\qquad t = \tau
\end{aligned}
\tag{A.1}
$$

We let the system to evolve in a compact time domain $\mathbb{T} = [0, 1]$ such that $\tau \in \mathbb{T}$. Given an initial condition $x_0 \in \mathbb{R}$, the solution x_1 can be obtained as follows

$$
\begin{aligned}
x_\tau &= e^{a\tau} x_0 && \text{1. integrate 1st flow until } t = \tau \\
x_\tau^+ &= cx_\tau = ce^{a\tau} x_0 && \text{2. at } t = \tau \text{ apply jump} \\
x_1 &= e^{b(1-\tau)} x_\tau^+ = ce^{b(1-\tau)} e^{a\tau} x_0 = ce^{a\tau + b(1-\tau)} x_0 && \text{3. integrate 2nd flow from } t = \tau \text{ to } t = 1
\end{aligned}
\tag{A.2}
$$

Alternatively, we can compactly write the solution at any time $t \in \mathbb{T}$ as

$$
x_t = \begin{cases} e^{at} x_0 & t < \tau \\ ce^{a\tau + b(t-\tau)} x_0 & t \geq \tau \end{cases}
\tag{A.3}
$$

Using the previous equation we can compute the gradient of solutions w.r.t. the parameters $a,\ b,\ c,\ \tau$. In particular, we have

$$
\begin{aligned}
\frac{\mathrm{d}x_t}{\mathrm{d}a} &= \begin{cases} te^{at} x_0 & t < \tau \\ \tau k e^{a\tau + b(t-\tau)} x_0 & t > \tau \end{cases} \\
\frac{\mathrm{d}x_t}{\mathrm{d}b} &= \begin{cases} 0 & t < \tau \\ (t-\tau) k e^{a\tau + b(t-\tau)} x_0 & t > \tau \end{cases} \\
\frac{\mathrm{d}x_t}{\mathrm{d}c} &= \begin{cases} 0 & t < \tau \\ e^{a\tau + b(t-\tau)} x_0 & t > \tau \end{cases} \\
\frac{\mathrm{d}x_t}{\mathrm{d}\tau} &= \begin{cases} 0 & t < \tau \\ (a-b) k e^{a\tau + b(t-\tau)} x_0 & t > \tau \end{cases}
\end{aligned}
\tag{A.4}
$$

Now let us consider a loss function computed on the mesh solution points of the trajectory

$$
L = \sum_{k=1}^{K} \gamma(x_{t_s}), \qquad 0 < t_1 < \cdots < t_S < 1,\ t_s \neq \tau
$$

of which we wish to obtain the minimizers $a^*,\ b^*,\ c^*,\ \tau^*$ via e.g. application of gradient descent methods. The gradient of the cost function w.r.t. any of the parameters $\theta \in \{a, b, c, \tau\}$ is given by

$$
\frac{\mathrm{d}L}{\mathrm{d}\theta} = \sum_{k=1}^{S} \frac{\mathrm{d}\gamma(x_{t_s})}{\mathrm{d}x} \frac{\mathrm{d}x_{t_s}}{\mathrm{d}\theta}.
$$

Simultaneous estimation of both the optimal dynamic parameters $a^*,\ b^*,\ c^*$ and a randomly initialized event time τ^*, will result in gradients of certain parameters to vanish or be completely incorrect.

Specifically, we note that parameter τ determines, beyond the specific time when the jump event occurs, also which parameters are responsible for computation of solution points x_{t_s}. Consider

the following two scenarios, where mode 1 is the first vector field of (A.1) and 2 is the second (post–event):

(1) Initialization of τ is an over–estimation of τ^* at the beginning of training. If this is the case, for t_s such that $\tau > t_s > \tau^*$ the mode is missclassified i.e. should be 2, but is still 1 due to the delayed event time τ. The gradient w.r.t b of loss computed on solution points $x_{t_k}, \tau > t_s > \tau^*$ is then wrongfully set to zero.

(2) τ is an under–estimation of τ^*. The same reasoning applies, except that for $\tau^* > t_s > \tau$ the mode is misslassified to 2, although it should be 1. This, in turn, affects the gradients for b, which results different than 0 despite the fact that b, from (A.1) should not be affecting the solution at points $t_s < \tau^*$. Any value taken by this gradient is thus incorrect, and can greatly affect the optimization procedure

We have shown how gradient pathologies exist even in the idealized linear case. In nonlinear systems with multiple events (including stochasticity) these effects can have a great empirical effect on a training procedure. The trajectory segmentation first approach of NHAs is designed to minimize their impact.

A.3 Extensions and Limitations

Automata reconstruction via symbolic regression NHAs with `categorical` encoders recover either a representation using the minimum number of modes necessary, corresponding to those of the system, or can be pruned due to immunity to mode mixing (discussed in Appendix B.3).

This property allows application of *symbolic regression* (SR) to reconstruct an analytic expression for each differential equation driving a system mode. This step grants domain experts a method to validate and certify the results, and enables construction of a human–readable automata representation for the SHS.

Clustered SR results can be improved by leveraging the *universal differential equation* approach employed in example by [10] for unimodal differential equations, by utilizing the decoder F_z as an *interpolating* source of additional trajectory data for each mode.

Latent hybrid automata from observations Learning methods for dynamical systems often introduce structure in latent space to enable control and identification from raw observations [41], [42]. Practical application for hybrid systems, such as robotic manipulation [43], locomotion [44], and traffic networks [2], might benefit from learning models structurally equipped with latent NHAs.

Optimal design of NHA modules for latent applications remains a difficult open question, as the analysis of deep models with latent spaces designed to evolve in continuous–time is also in its infancy.

Unified benchmark for model development Despite the importance of hybrid systems in engineering, wide differences in techniques across domains have historically made it difficult to develop and preserve a unified set of benchmarks.

Evidence from other deep learning disciplines e.g. computer vision highlights the importance of consistent and curated benchmark datasets to track and measure the impact architecture and method optimizations. We argue further benchmark design, along with larger datasets, to be a necessary step required to trigger an `ImageNet`–like [45] moment for general neural differential equations and thus also NHAs. As an additional challenge, we note that performance of continuous neural models is in general highly impacted by the numerical method used for forward and backward inference, with optimal methods usually system or application dependent. This makes decoupling architecture improvements from the numerical underpinnings harder than for traditional models.

A.4 Detailed Feature Comparisons with Related Work

Table 3 compares the proposed method with recent learning based approaches in terms of features. We use ✗ for features that are either absent or incompatible with a given method, or features that have not been tested or verified, although the method itself may be adapted to include it.

We consider the following:

- **Recovery of flows and events:** can state–space vector fields be learned along with the events. In [11], learned *latent* dynamics aid in the intensity parametrization of the point process. State–space dynamics are not learned simultaneously with point process maximum likelihood training. [13] trains a neural network vector field along with a parametrized event function.
- **Stochastic events:** has the method been shown to be compatible with stochastic events. The formulation of [13] can parametrize stochastic events via inverse sampling, but no experiments have been performed, likely due to difficulties in learning stochastic events from a full trajectory.
- **Mode identification:** does the method recover modes of a multi–mode hybrid system, and can the vector field approximate a different dynamics for each. NHAs are the first method to tackle this setting.
- **Adaptive end–time:** can the method adjust event times by calculating gradients with respect to integration end–times. Core contribution of [13] is an implicit differentiation formulation to adapt end-times. While adaptive segmentation has been discussed as being compatible with NHAs, no targeted experiments on this technique have been carried out. The extension is left as future work.
- **Intensity–free parametrization:** does the method use intensity–free parametrizations to avoid numerically solving integrals to sample from next–event densities. [11], [13] parametrize the intensity as only a single mode is considered. NHA use normalizing flows to approximate these densities directly, since intensity parametrization scale poorly as the number of system modes increases.

A.5 Broader Impact

This work represents a first attempt in developing a data–driven, learning based technique for *stochastic hybrid system* (SHS) identification and control. As discussed in the main text, existing methods currently rely on strict assumptions that severely limit their utilization in practice. Applications domain the SHS formalism provides an accurate language to describe a target system are most likely to be affected by the availability of NHAs as a method to improve partial mathematical models using data or construct from scratch a model of the system and its automata representation. The impact of NHAs here is thus likely to be similar in scope to the impact of neural differential equations in science and engineering.

We do not anticipate significant negative environmental impact from the adoption of NHAs as these models are still orders of magnitude smaller than other large deep learning architectures for domains such as natural language.

B   Experimental Details

Hardware and software resources   Experiments have been performed on a workstation equipped with a 48 threads AMD RYZEN THREADRIPPER 3960X, a NVIDIA GEFORCE RTX 3090 GPUs and two NVIDIA RTX A6000. All models and datasets fit in a single GPU. The software implementation of NHA leverages the `PyTorch` framework. ODE solvers and numerical methods for hybrid systems have been developed from scratch and are included in the submission.

Common experimental settings   In all experiments, unless specified, the NHA mode encoder $\mathcal{E}_\theta$ is capped with a `softmax` activation computing the probabilities of a categorical distribution from which then the one–hot mode z is sampled.

Method	Recovery of flow + events	Stochastic events	Mode identification	Adaptive end–time	Intensity–free parametrization
NJSDE [11]	✗	✓	✗	✓	✗
Neural Event ODE [13]	✓	✗	✗	✓	✗
NHA (this work)	✓	✓	✓	✗	✓

Table 3: Feature comparison between neural models for hybrid systems. ✗ is used to indicate features that are either not compatible, or have not been verified in the original work.

Simulation Hyperparameter	Value
Number trajectories	40
ODE solver	Dormand-Prince
Tolerances (abs, rel, event)	$10^{-6}, 10^{-6}, 10^{-4}$
τ_{off}	3
η	1
n_{ack}	2
p_{drop}	0.05
κ	4

Training Hyperparameter	Value
Training iterations (mode recovery)	4000
Encoder $\mathcal{E}_\theta$ learning rate	$5 \cdot 10^{-4}$
Decoder F_z learning rate	10^{-2}
Optimizer	Adam
$\mathcal{E}_\theta$ layer dimensions	$[\cdot, 64, 65, 64, m]$
$\mathcal{E}_\theta$ activation	ReLU
$\mathcal{E}_\theta$ dropout	$[0.3, 0.3, 0.3]$
F_z layer dimensions	$[2 + m, 2]$
Training iterations (event training)	4000
Learning rate	$2 \cdot 10^{-3}$
Optimizer	Adam
$\psi_{z \to z'}$ layer dimensions	$[2, 32, 2]$

Table 4: Hyperparameters of **[Left]** TCP data simulation **[Right]** NHA in the TCP experiment, mode recovery and event module training.

Gradients through the sampling operation are computed via *straight–through–estimation* (STE) [27], which can be implemented with a stop_gradient (e.g. detach in PyTorch) operation present in modern deep learning frameworks. Let z be the one–hot representation of system mode, and p a vector of probabilities for the corresponding categorical distribution, computed as output of a neural network parametrized NHA encoder $\mathcal{E}_\theta$. STE can be realized in a single line as $z - p.\texttt{stop\_gradient}() + p$. STE ensures the output of the encoder $\mathcal{E}_\theta$ is strictly one–hot encoded, while simultaneously ensuring that the gradients backpropagate directly through the probabilities.

The data–controlled Neural ODE decoder F_z incorporates mode information to select

$$\dot{x} = \sum_{i=1}^{m} z_i \; f_i(t, x, \omega_i)$$

where z is one–hot encoded, and thus only a single neural network vector field f_i with parameters ω_i determines the solution.

B.1 Identification of Reno TCP

Experimental setup Tables 4 provide hyperparameters for data simulation and training of NHA. Unless otherwise specified simulation, training and testing is repeated for 10 different random seeds.

The complete experiment on learning the Reno TCP system involves multiple stages: (i) mode recovery and (ii) training of the NHA event module. As baselines for (i), we consider several Neural ODE variants similar to NHA decoder F_z, with latent z obtained in different ways. Latent Neural ODEs obtain z as sampled for Normal distribution $\mathcal{N}_\theta := \mathcal{N}(\mu_\theta, \sigma_\theta)$ parametrized by a neural network matching the architecture of $\mathcal{E}_\theta$. Reparametrization is used to backpropagate through the sampling procedure. *Data–controlled Neural ODEs* (DC–NODEs) are comparable to Latent Neural ODEs model with the major difference in the computation of latents as $z = g_\theta(X)$ with g_θ once again matching $\mathcal{E}_\theta$. All decoders F_z are equivalent, except in the case of Augmented Neural ODEs (the Neural ODEs is zero–augmented [9] i.e. $z := 0$) where the absence of the encoder is balanced by a more expressive decoder with three–layers. The normalizing flows $\psi_{z \to z'}$ in NHA event modules are designed as spline flows [32] with two layers. We use the standard implementation of spline flows in Pyro [46].

During mode recovery, all models are trained on 5–folds of 5. Training is performed by parallel integration across subtrajectories X_i using the Runge-Kutta4 explicit solver. All gradients are computed via reverse–mode automatic differentiation. We test models with lowest cross–validation reconstruction MSE loss, since cross–validation v–score would not be available without ground–truth labels. We find that lowest reconstruction loss often correlated with best v–measure. Baselines for mode clustering (ii) include standard clustering algorithms k–means++ [29], hierarchical [30] and DBSCAN [31]. We use scikit-learn [47] implementation of all baseline algorithms. We perform light hyperparameter tuning on ground–truth labels for k–means++ and hierarchical to optimize their

performance in the range $m \in [3, 5, 10]$. DBSCAN is similarly tuned to optimize its performance with parameter ϵ indicating the maximum size of neighbourhoods around a data point. Subtrajectories classified as noise by DBSCAN are counted as incorrectly clustered.

We observe DBSCAN performance to be correlated to NHA self–supervised mode recovery. Both methods excel when density of data points under some metric is indicative of cluster separation. However, NHA self–supervision relies on the additional inductive bias of data points in a subtrajectory representing observations of a solution of an ODE, whereas DBSCAN does not. The denser the trajectories, the more restricting the Neural ODE representation limitations, and the easier each cluster is to find. Due to the similarity in their working principle, DBSCAN performance can be used as a quick sanity check to determine whether the dataset is suitable to NHA mode recovery.

B.2 Robustness to Segmentation Noise

We investigate robustness of NHA mode recovery and related baselines to a noisy segmentation in subtrajectories X_i. To simulate incorrect segmentations, we collect segmentation indices and perturb them by adding or removing an uniformly sampled from $[1, 10]$. Each index has a p probability of being corrupted by noise, and we repeat mode recovery with $p \in [0.1, 0.3, 0.5]$ (3 times per p). Shifting left or right by values sampled from $[1, 10]$ results in significant data corruption; certain subtrajectories, being shorter than 10 points, can be completely absorbed into a different subtrajectory. Table 5 reports the differences in v–measure compared to the results of Section 5.1. For each baseline, we report best results in terms of hyperparameter $m \in [3, 5, 10]$, typi-

	Δ		
Model	$p = 0.1$	$p = 0.3$	$p = 0.5$
k–means++	-0.01 (0.29)	-0.05 (0.25)	-0.08 (0.22)
hierarchical	-0.00 (0.31)	-0.02 (0.29)	-0.03 (0.28)
DBSCAN	-0.08 (0.61)	-0.28 (0.41)	-0.46 (0.23)
NHA–3	$+0.02$ (0.88)	-0.13 (0.73)	-0.45 (0.41)
NHA–5	-0.00 (0.91)	-0.17 (0.74)	-0.48 (0.43)
NHA–10	-0.07 (0.89)	-0.25 (0.71)	-0.41 (0.45)

Table 5: v–measure performance differences after self–supervised mode recovery performed on a dataset with imperfect segmentation noisy segmentation of the TCP dataset of the main text. We evaluate each method under an increasing degree of data corruption. Hyper-parameter p indicates the probability for a subtrajectory X_i to be subject to a noisy segmentation i.e. to have the index determining its initial condition be perturbed and shifted either left (before) or right (after). In parenthesis, the v–measure of each model in a given noisy regime.

cally $m = 10$, corresponding to $\epsilon = 1$ for DBSCAN. Although specific perturbation patterns may affect the model more than others, the trend uncovered by the results is clear.

B.3 Switching Linear System and Mode Mixing

Experimental setup   We considered the two–dimensional switching linear system reported in [20], described by the dynamics

$$(\dot{x}_t, \dot{y}_t) = f(x_t, y_t) := \begin{cases} (-y_t, x_t + 2) & \text{if } x_t \geq 2 \\ (-1, -1) & \text{if } x_t < 2 \wedge y_t \geq 0 \\ (1, -1) & \text{if } x_t < 2 \wedge y_t < 0 \end{cases} \quad \text{(B.1)}$$

We performed an ablation study on the effect of the categorical sampling for the mode selection in NHAs in presence of redundant "free" modes. In particular, we considered the following learning model

$$(\dot{x}_t, \dot{y}_t) = \sum_{i=1}^{4} w_t^i f_i(x_t, y_t) \quad \text{(B.2)}$$

with one redundant mode. F_i ($i = 1, 2, 3, 4$) was two-layers neural networks with 32 neurons each, `softplus` activation on the first hidden layer and hyperbolic tangent activation on the second one. We then defined two variants of the model: a first variant with $w_t = (w_t^1, w_t^2, w_t^3, w_t^4)$ directly obtained via `softmax` normalization of the output of a neural network g,

$$w_t = \texttt{softmax} \, g(x_t, y_t);$$

18

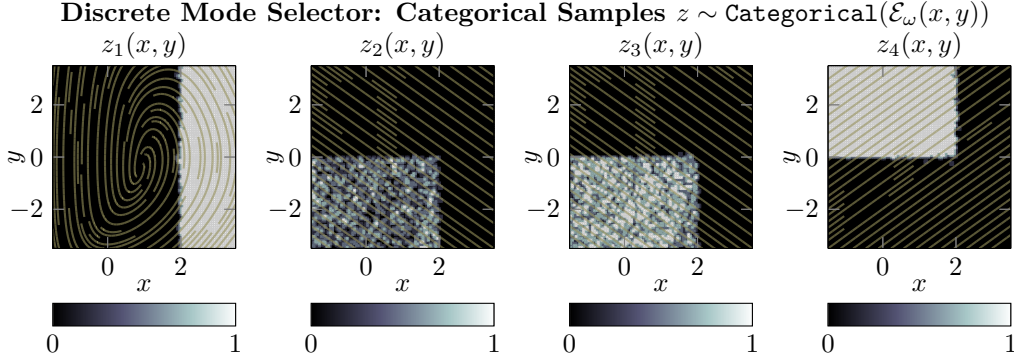**Discrete Mode Selector: Categorical Samples** $z \sim \texttt{Categorical}(\mathcal{E}_\omega(x,y))$

Figure 10: Reconstructed conditional vector fields F_z and corresponding mode classification boundaries. The `categorical` encoder uses two identical modes for a single ground–truth vector fields.

and a second one where w_t is obtained by a categorical sample conditioned by $g(x_t, y_t)$, i.e.

$$\forall t \quad w_t \sim \texttt{categorical}(\texttt{softmax}\, g(x_t, y_t))$$

g was fixed as a neural network made up by two layers with 64 units and `SiLU` (`swish`) activation. The two models were trained on a L_1 reconstruction loss of nominal trajectories of the system (B.1). We introduced a regularization term penalizing the squared error on un–normalized finite differences of nominal/reconstructed trajectories as a proxy for the vector field information.

Mode pruning Uniqueness theorems for ODE solutions guarantee that, given an initial condition and a mode latent code z, the decoder F_z will always produce the same trajectory. Immunity to mixing for categorical latents enables mode pruning and recovery of a minimal representation. If $\mathcal{L}_r$ saturates, the encoder has not been initialized with a sufficient number of modes m. Redundant modes may be pruned, in example, by merging them if a similarity measure between the corresponding vector fields F_{z_i}, F_{z_j} e.g. difference in a given norm calculated on data trajectories, is *small enough*. Figure 10 provides an example result of the second scenario discussed in Section 5.2, where `categorical` NHA encoders use more than a single latent mode for a target underlying mode. However, due to their immunity to mode mixing, the vector fields are equivalent, and can be merged. We show this in Figure 9, where the L1–norm between F_2 and F_3 is shown to be small in the region where the corresponding modes 2 and 3 are active.
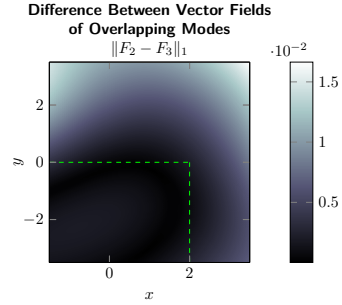

Figure 9: Similarity between learned mode vector fields F_2 and F_3 of Figure 10. The two vector fields are equivalent in the region of interest, as indicated by the L1–norm, and the corresponding modes can thus be merged.

B.4 End–To–End Learning of Hierarchical Controllers for Dynamical Systems

Experimental setup Our objective is to control a swarm of differential drive robots moving on a planar space. The system dynamics are

$$
\begin{aligned}
\dot{x}_1 &= u_v \cos\theta \\
\dot{x}_2 &= u_v \sin\theta \\
\dot{\vartheta} &= u_r
\end{aligned}
\tag{B.3}
$$

where ϑ is the orientation of a single robot. The control $[u_v, u_r] \in \mathbb{R}^2$ is obtained via the low–level, time–invariant feedback controller $u_z := u(x_1, x_2, \vartheta, z)$, with z produced and switched every 5 seconds by the planner. Both the controller and the policy π, are parametrized by a neural network. We use `Adam` for both networks, with learning rates $10^{-3}, 10^{-3}$.

The training of low–level controller u_z and high–level planner π is carried out concurrently. We perform batch training on robot swarms of $N = 80000$. At the beginning of each episode, we sample

the initial conditions uniformly in a square region, with each robot rotated according to a random orientation also uniformly sampled in $[0, 2\pi]$. During each episode, we simulate the switching and control behaviour of each robot with respect to two pre-defined map layouts, both shown in the alternating resource pattern of the upper-left plot of Figure 8a. Each map layout has $M = 5$ resource locations, where two auxiliary scalar variables r_1 and r_2 specify, for each resource, its planar location.

We train policy networks $\pi(x_1, x_2, r_{11}, r_{21}, ..., r_{1m}, r_{2m})$ where the inputs correspond to the concatenated robot states, together with the flattened resource locations. The $M-$dimensional softmax output determines a categorical probability distribution over the resources is then used to sample a resource target.

A reward can be assigned to each robot based on the ability to select the correct target. For each robot, we generate a reward of 1 if the selected target is correct, and 0 otherwise. Let $G(s_i, p_i)$ be the reward of robot i in the swarm, we can compute the reward for a swarm in a map by $R = \sum_i^N \frac{G(s_i, p_i)}{1000}$ where s is the categorical sample from the distribution over the targets, and p are the reference targets computed by $\arg\min_j ||[r_{1j}, r_{2j}] - [x_1, x_2]||$ (note $R \in [0, 80]$ for any one episode), with x_1, x_2 being the robot location at the time of switching. The target selector is trained by minimizing a $\mathcal{L}_\pi = -\frac{1}{T} \sum_t^T ln(\pi(s_p^{(t)}) * R)$, where T is the number of alternating maps, and $s_p^{(t)}$ denotes the concatenated robot location and resource map with respect to the tth map layout used for training.

The target selected by the planned informs low–level controller u_z via the corresponding resource location. In particular, we provide as input to u_z the coordinates $z := [r_1, r_2]$ of the target chosen by π. This augmented state is used by u_z to resolve the robot's dynamics and drive the swarm closest to their selected targets. We train u_z by solving a continuous–time optimal control problem with a terminal RMSE loss between the state reached by the robot and the objective set by the policy planner. Here, we integrate the system using the adaptive–step `DormandPrince` [48] solver with tolerances $10^{-3}, 10^{-3}$.

Discussion of results   Figure 8 shows the average reward and control loss of the robot swarm during training, with both trends converging after 4000 episodes. Figures 8a and 8b show the generated control of a randomly generated swarm of 100 robots on two new maps. In the first map, the targets consist on alternating patterns of the learned map layouts, generating a straight line pattern which correctly captures the greedy robot policy imposed. The second map consists instead of a new, unseen, map layout within the alternation. The trained model is capable of generalizing the planning and control strategy to account for the new map layout, by redirecting the robots onto their closest resource in a wave-like pattern. On the first tested map, the model achieves $99.8\% \pm 0.8\%$ average target accuracy for the 100 robot tested batch. On the second tested map, the model achieves $98.5\% \pm 1.95\%$ average target accuracy for the 100 robot tested batch.

C   Realization of NHAs

C.1   Software Implementation of Hybrid Integration

We provide documented `Python` pseudo–code for the hybrid system adaptive integration algorithm used for dataset generation. This function can handle hybrid systems with multiple modes and transitions. Each possible event requires its own callback function with `check_event` and `jump_map` methods. We provide an example of one such callback under `odeint_hybrid`.

```python
def odeint_hybrid(vf, x, t_span, solver, callbacks, atol, rtol, event_tol):
    """ODE solver for hybrid systems with multiple events."""
    # initialize event state tracker, one boolean for each possible event
    # (or edge in the automata representation of the SHS).
    event_states = [False for _ in range(len(callbacks))]
    dt = initial_step_size(f, k1, x, t, solver.order, atol, rtol)

    while t < t_span[-1]:
        # tentative step
        x_step, x_err = solver.step(vf, x, t, dt)

        # check whether any event
```

```
13          # has been triggered in the interval [t, t + dt]
14          new_event_states = [cb.check_event(t + dt, x_step)
15                                      for cb in callbacks]
16
17          # has any event state moved from `False' to `True' in [t, t + dt]?
18              triggered_events = sum([(zp != z) & (z == False)
19                      for zp, z in zip(new_event_states, event_states)])
20          # if an event / mode transition has been triggered,
21          # find exact event time and state
22              if triggered_events > 0:
23                  x, t = root_find_event(max_iters, event_tol)
24
25                  # if there is a conflict and multiple events are triggered,
26                  # takes always the one with smaller ID
27                  zp = min([i for i, ev in enumerate(new_event_states)
28                              if ev == True])
29
30                  t = t + dt
31                  # save state and time BEFORE and AFTER jump
32                  sol.append(x)
33                  eval_times.append(t)
34
35                  # apply jump func.
36                  x = callbacks[zp].jump_map(t, x)
37
38                  sol.append(x)
39                  eval_times.append(t)
40
41          # when there are no events,
42          # proceed as usual with adaptive integration
43              else:
44                  error_ratio = compute_error(x_step, x_err, atol, rtol)
45                  accept_step = error_ratio <= 1
46
47                  if accept_step:
48                      t = t + dt
49                      sol.append(x)
50                      eval_times.append(t)
51
52                  else:
53                      dt = adapt_step(dt, error_ratio, safety,
54                                      min_factor, max_factor, order)
55
56      return eval_times, sol
```

The callbacks are in the form:

```
1  class EventCallback(nn.Module):
2          super().__init__()
3
4      def check_event(self, t, x):
5          raise NotImplementedError
6
7      def jump_map(self, t, x):
8          raise NotImplementedError
9
10
11 class StochasticEventCallback(nn.Module):
12
13          super().__init__()
14          self.exponential = Exponential(1)
15
16      def initialize(self, x0):
```

```python
17          # sample one `s' for each batch in x0, to identify events
18          # as described in Section 2. Exponential, instead of Uniform
19          # is used to avoid `log' computations.
20          # Should be sampled again after every event is triggered.
21          self.s = self.exponential.sample(x0.shape[:1])
22
23      def check_event(self, t, x):
24          raise NotImplementedError
25
26      def jump_map(self, t, x):
27          raise NotImplementedError
```